Rational Design of Bioinspired Nanocomposites with Tunable Catalytic Activity

Hans C. Hendrikse, Alejo Aguirre, Arno van der Weijden, Anne S. Meeussen, Fernanda Neira D'Angelo*, Willem L. Noorduin*

Supporting Information

S1. Growth of $BaCO_3/SiO_2$ nanocomposites

$BaCO_3/SiO_2$ nanocomposites on a substrate were prepared as described in previous literature.[28] In short, a substrate (e.g. 2x2 cm slide of aluminum, glass or silicon) was vertically positioned in a 100 mL beaker containing $BaCl_2$ dihydrate (74 mg, 0.3 mM) and Na_2SiO_3 (16 mg, 0.13 mM) dissolved in 15 mL of water. The reaction vessel was loosely covered with a Petri dish to allow CO_2 from the air to slowly diffuse into the reaction mixture. Typical growth times ranged between 1.5-2.0 hours after which the substrate was removed from the solution and washed with deionized water and the resulting $BaCO_3/SiO_2$ nanocomposites were converted into $Co(CO_3)_x(OH)_{2-2x}/SiO_2$ nanocomposites instantly after this. The composition of the nanocomposites was determined using SEM, EDS and XRD as shown in Figure 2 (A, B, and C respectively). The used reference for the XRD-diffractogram can be found in the Crystallography Open Database (COD 1000033).

S2. Scaled up growth of $BaCO_3/SiO_2$ nanocomposites

A solution of $BaCl_2$ (7.4 g, 30 mM) in 300 mL of water was added to a solution of Na_2SiO_3 (1.6 g, 13 mM) in 1200 mL of water. This solution was shortly stirred and poured in a metal tray (30x50x10 cm) to maximize the surface area in contact with air, while keeping at least 1 cm of depth to the solution. The solution was left for 1,5 hours with the tray covered with a perforated cardboard lid. The resulting nanocomposites floating on the meniscus were separated from the solution via vacuum filtration. For further exchange reactions, the microstructures were instantly removed from the filtration paper with a spatula and transferred directly into the exchange solution.

S3. Exchange to amorphous $Co(CO_3)_x(OH)_{2-2x}/SiO_2$ nanocomposites

Cobalt nitrate hexahydrate ($Co(NO_3)_2$) (727 mg, 2.50 mM) was dissolved in 50 mL of demineralized water. A substrate containing $BaCO_3$ microstructures was placed in this solution for 50 minutes. Afterwards, the substrate containing the purple nanocomposites was removed and washed in two demineralized water baths followed by an acetone bath. Full exchange while preserving shape was determined with EDS and SEM respectively. XRD showed amorphous material had formed (see Figure 2), rather than the expected $CoCO_3$ crystal structure found in the Crystallography Open Database (COD 1548825). IR-spectroscopy confirmed that indeed an amorphous basic carbonate had formed (see Figure S10).

S4. Scaled up exchange to amorphous $Co(CO_3)_x(OH)_{2-2x}$ /SiO_2 nanocomposites

Cobalt nitrate hexahydrate ($Co(NO_3)_2$) (11.6 g, 40 mM) was dissolved in 200 mL of demineralized water. $BaCO_3/SiO_2$ nanocomposites were transferred from a filtration paper into this solution using a spatula, while gently stirring the solution to spread the nanocomposites. Afterwards, the resulting purple nanocomposites were separated from the solution using vacuum filtration and washed with demineralized water followed by acetone. Full exchange was determined with EDS, while XRD showed an amorphous $Co(CO_3)_x(OH)_{2-2x}$ phase had formed as was the case with the conversion on a substrate.

S5. Decomposition to Co_3O_4/SiO_2 nanocomposites (normal and scaled up)

Amorphous $Co(CO_3)_x(OH)_{2-2x}/SiO_2$ nanocomposites were placed in an open single zone tube furnace and heated to 650 °C for 4 hours, to obtain a crystal size of ca. 17 nm. Changing this elevated temperature results in different crystal sizes, with exclusively heating to temperatures of 530, 560, 590 and 620 °C for 4 hours results in crystal sizes of ca. 10, 12, 14, and 15 nm respectively (see Figure 3B and Table S1). The resulting black nanocomposites were determined to be composed of Co_3O_4 by XRD, with preservation of microshape and metal to silicon ratio of 4:1 as shown by SEM and EDS respectively (Figure 2C). The used reference for the XRD-diffractogram can be found in the Inorganic Crystal Structure Database (ICSD 27498).

S6. Scanning electron microscopy (SEM) and energy-dispersive X-ray spectroscopy (EDS) characterization

Samples were loaded into the SEM without applying a conductive metal coating. SEM images were obtained using a FEI Verios 460 equipped with an Everhart-Thornley detector (ETD) and a circular backscatter detector (CBS). The images were recorded at 10 kV using a 100 pA current in both instances. EDS was measured with the same electron microscope using an Oxford X-Max^n energy dispersive X-ray spectrometer with an accelerating voltage of 20 kV, using a 100 pA current.

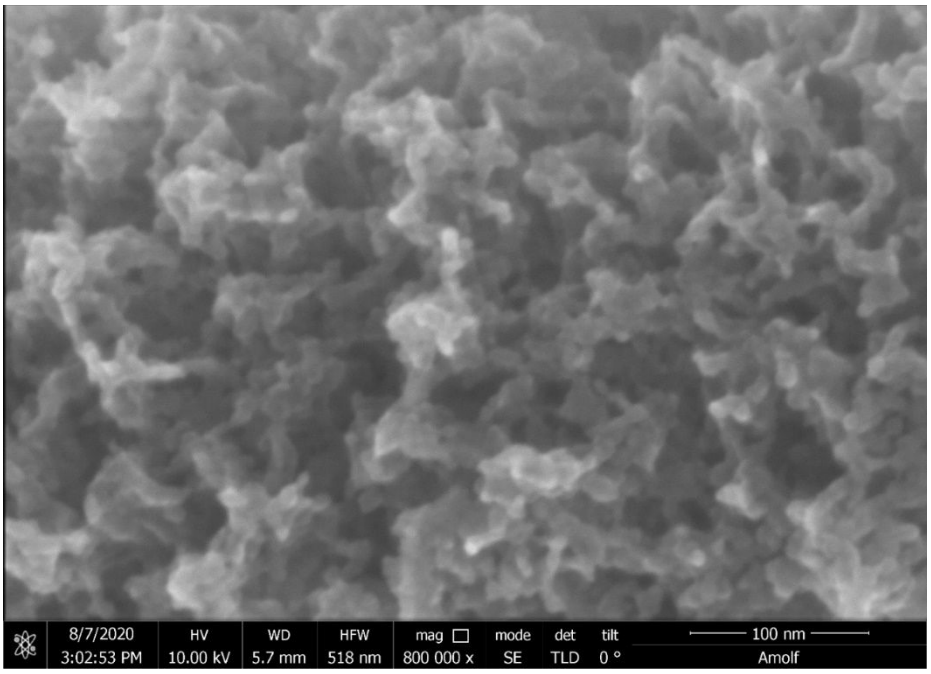

Figure S1. Magnified version of Figure 1D (without EDS overlay), showing the individual nanocrystals and porous nature of the surface of a nanocomposite.

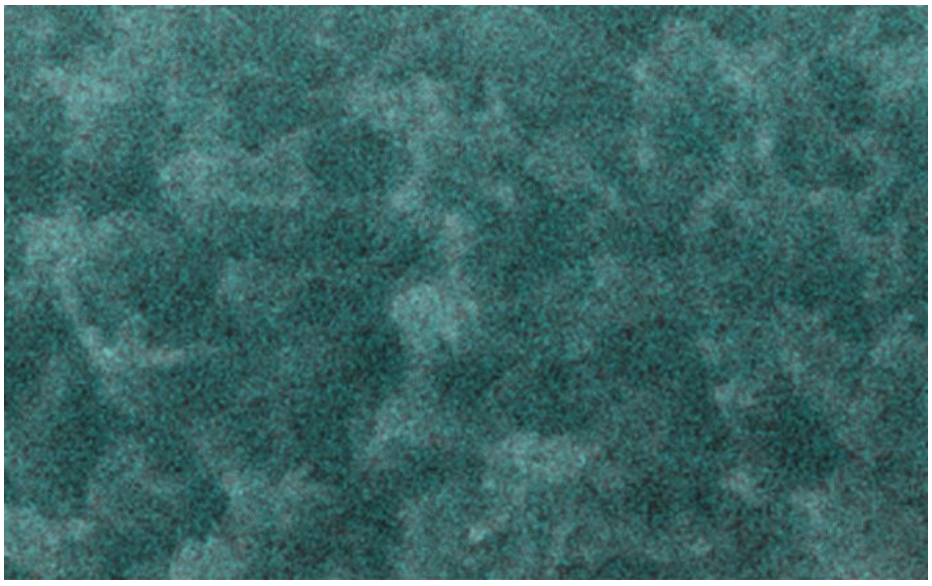

Figure S2. Magnified version of Figure 1D (with EDS overlay), showing the uniform dispersion of cobalt in cyan.

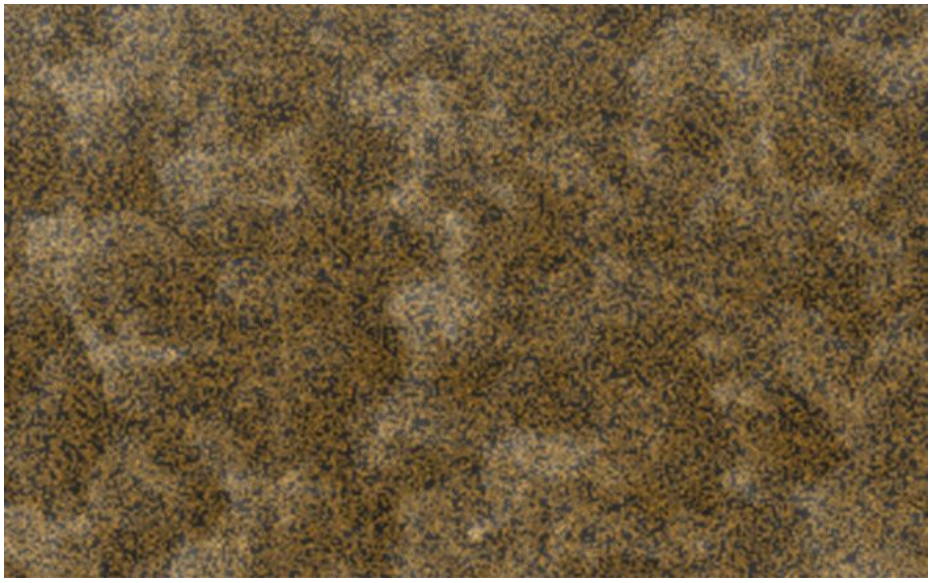

Figure S3. Magnified version of Figure 1D (with EDS overlay), showing the uniform dispersion of silicon in brown.

X-ray diffraction (XRD) characterization

S7. X-ray diffraction (XRD) characterization

X-ray diffraction measurements were performed using a Bruker D2 Phaser (Bragg-Brentano geometry) using a K-alpha Cu X-ray source with an emission energy of 8.0415 keV. The samples were mounted inside a chamber filled with ambient air at room temperature. All measurements were performed using a 2.0 mm beam knife to reduce unwanted scattering and optimize the low angle part of the diffractogram. A nickel filter was used to reduce the 20-30% contribution from the k-beta Cu X-ray source. A divergence slit of 0.6 mm was used to control the illuminated area of the sample, based on the available material. Diffracted X-rays were detected using a Lynxeye detector and were collected for at least 12 hours with a scan interval ($\Delta 2\theta$) of 0.01°, or 0.004° for individual peaks. Diffractograms were calibrated using reference spectra mentioned in the preparation of each material. It should be noted that in general nanocomposites grown on the meniscus were used for this analysis, rather than structures grown on a substrate to maximize the signal to noise ratio in the XRD measurement.

S8. Crystal size determination from XRD patterns

The crystal domain size at various decomposition temperatures T was determined using XRD. The [311] peaks of five Co_3O_4 nanocomposites, obtained with the preparation methods described in this article, were measured. Debye-Scherrer theory (A.L. Patterson, *Phys. Rev.*, **1939**, 56, 987-982) relates the crystal domain size τ to the full width at half maximum (FWHM) β of spectral peaks via

$$\tau = \frac{K\lambda}{\beta \cos\theta_p}$$

where K is a material-dependent shape factor that is estimated at 0.9 given the material's cubic symmetry (J.I Langford and A.C.J. Wilson, *Journal of Applied Crystallography*, **1978**, 11, 102-113) , $\lambda = 0.154060$nm the incident wavelength, and θ_p the peak angle.

The experimental data (Figure S4A-B) show a Lorentzian peak (J.I Langford, D.Louër, *Report on Progress in Physics*, **1996**, 59, 131-234) of amplitude I_{max} with a linear offset $2B\varphi + C$, which we fit numerically with the model:

$$I_{max} = \frac{\left(\frac{\beta}{2}\right)^2}{\left(\frac{\beta}{2}\right)^2 + (2\varphi - 2\theta_p)^2} + 2B\varphi + C$$

Least-squares fitting via a custom Python script yields estimates for θ_p and β, as well as their errors in the form of a covariance matrix. Ignoring correlations, the square roots of the matrix' diagonal entries form lower bounds for the standard errors $\Delta\theta_p$ and $\Delta\beta$, which yield a minimal standard error

$$\sqrt{\left(\frac{\Delta\beta}{\beta}\right)^2 + (\Delta\theta_p tan\theta_p)^2}\tau$$

on the domain size via established uncertainty propagation methods (Figure S4C, H.H. Ku, *Journal of research of the national bureau of standards C*, **1966**, 70, 263-273). Reducing the signals' white Gaussian noise level with various filtering methods does not lead to significantly different domain size estimates (Figure S4D).

In the case of the nanocomposites heated to 530 °C, the calculated crystal domain size of $\tau = 9.9 \pm 0.5$nm is in good agreement with the observed size in the high-resolution SEM image of Figure 1B. The crystal size for the other decomposition temperatures was determined in a similar fashion. Table S1 summarizes the results, while Figure S4 shows the used fits and peaks.

Decomposition Temperature (°C)	**Crystal Size (nm)**
530	9.9 ± 0.5
560	12.2 ± 0.3
590	14.4 ± 0.3
620	15.1 ± 0.4
650	17.2 ± 0.3

Table S1. Obtained Grain Sizes using different decomposition temperatures.

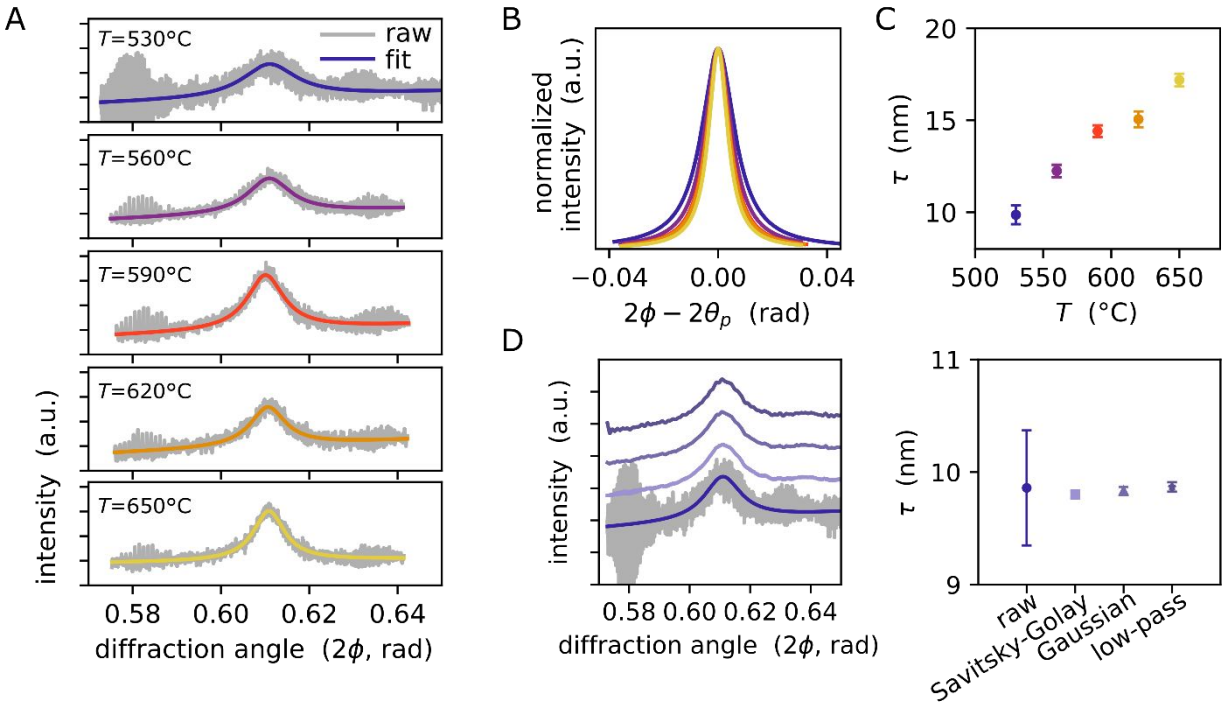

Figure S4. Full width half maximum determination of [311] peak of Co_3O_4, heated to **A.** T = 530 to 650°C. Gray lines show the original diffractogram and coloured lines the fit used to determine crystal size. **B.** Overlay of normalized fits obtained in A, with linear offset subtracted. **C.** Grain sizes τ measured at various decomposition temperatures. **D.** Left: noise reduction on raw data (gray line, T = 530°C) with Savitsky-Golay, Gaussian, and low-pass filters (colours; offset added for clarity) do not lead to significantly different fitted grain sizes (right).

S9. Microshape shrink calculation

The volume change is calculated based on the SEM images of $BaCO_3/SiO_2$ and Co_3O_4/SiO_2 (Figure 2A). We measure the length and width of each extrusion perpendicular to the viewing angle in the SEM image and compute the volume of the architecture by taking into account that the coral-like forms are almost perfectly half-spherical. In these calculations, only the extrusions which lay perpendicular to the viewing direction are used, to avoid errors derived from projecting a 3D object on a 2D plane. The volume change is computed by comparing the volumes of the same architecture before and after conversion (Figure S5), where the volume ratio is assumed to be equal to the length ratio multiplied by the width ratio squared.

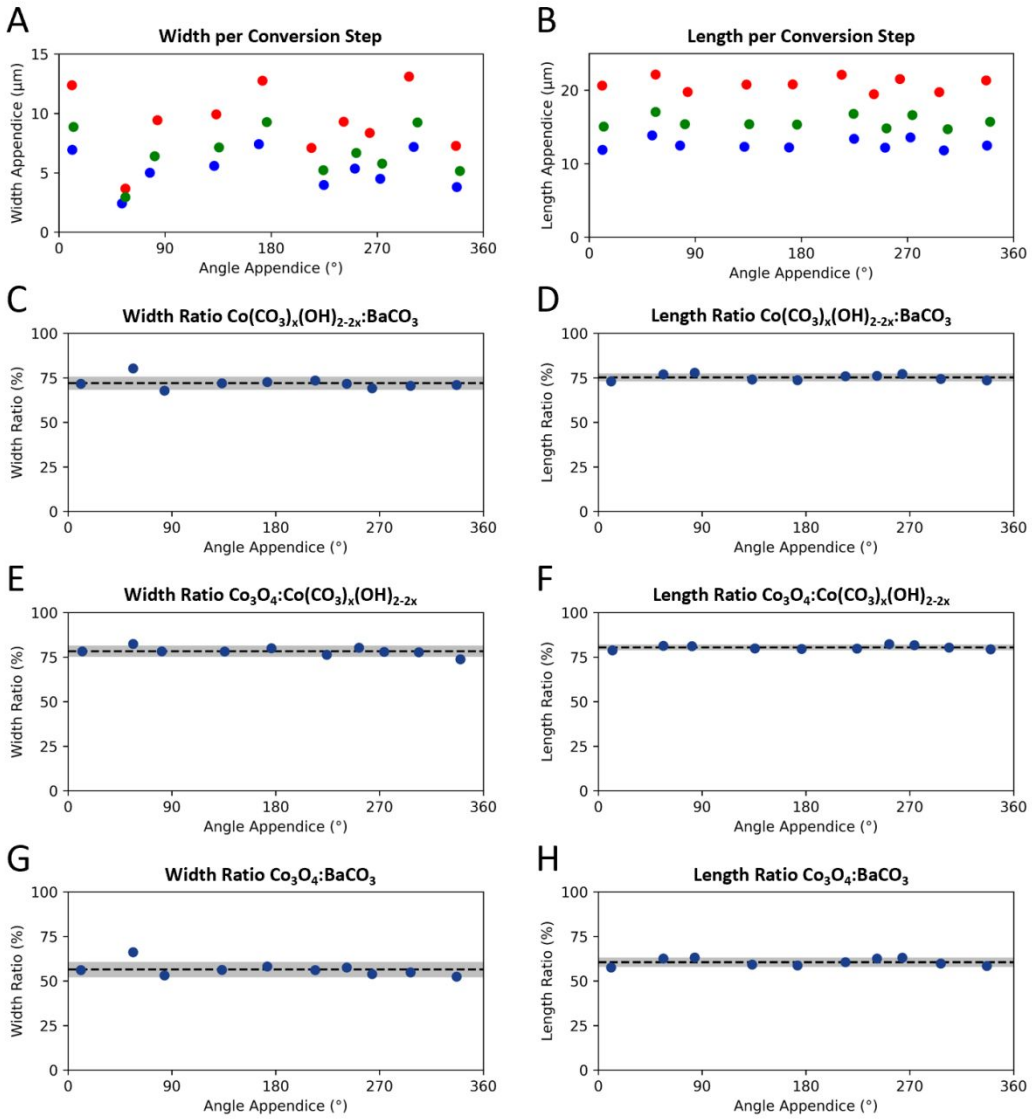

Figure S5. A. Widths and **B**. lengths of nanocomposite appendices before ($BaCO_3/SiO_2$, red) and after the first ($Co(CO_3)_x(OH)_{2-2x}/SiO_2$, green) and second ($Co_3O_4/SiO_2$, blue) conversion**.** The resulting after/before ratio (blue: individual appendices, dashed line: mean, grey zone: standard deviation) for the width and length are plotted respectively for **C**, **D**. the conversion from $BaCO_3$ to $Co(CO_3)_x(OH)_{2-2x}$, **E**, **F**. the conversion from $Co(CO_3)_x(OH)_{2-2x}$ to Co_3O_4 and **G**, **H**. the overall conversion. The x-axis in all instances displays the clockwise angle of the appendices in relation to the y-axis.

S10. TEM Measurements

The 17 nm Co_3O_4/SiO_2 nanocomposite samples were analyzed by scanning TEM (STEM) CryoTitan (FEI), using a High Angle Annular Dark Field Scanning Transmission Electron Microscopy (HAADF-STEM) at room temperature. STEM images were acquired using a probe convergence angle of 10 mrad, a dwell time of 2µs and a camera length of 89 mm in combination with a Fischione HAADF STEM detector.

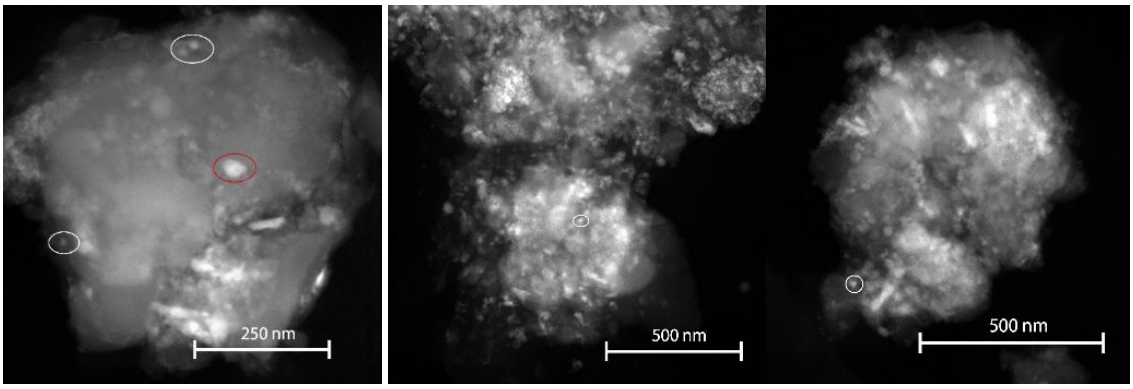

Figure S6. HAADF STEM images of the Co_3O_4/SiO_2 nanocomposites. Lighter areas correspond to Co_3O_4 nanocrystallites while darker areas correspond to the SiO_2 support. A few examples of ca. 15-17 nm Co_3O_4 nanocrystallites are highlighted in white circles, and an example of a larger agglomerate of ca. 34 nm, likely formed by two Co_3O_4 crystallites, in a red circle.

S11. Scaling Setup

In order to scale the nanocomposite production, a tray rather than a beaker was used for their preparation. The co-precepitation was performed following the procedure described in Section S2. Figure S7 shows the difference in scale between the surface of the water-meniscus available in the tray (top) and the surface available on a substrate (bottom left). The growth on the meniscus in the tray yields roughly 500 times the amount of nanocomposites compared to the growth on a substrate. Afterwards, ion exchange reactions were performed as described in Section S4, while conversion towards the desired Co_3O_4 was performed as described in Section S5. The resulting composites can be converted with high conversion rates over 95%, as shown by EDS and XRD in Figure S8.

Figure S7. Photograph of the scale difference between growing the architectures in a tray (top) rather than on a substrate (bottom left). Ruler is 20 cm for reference (bottom right).

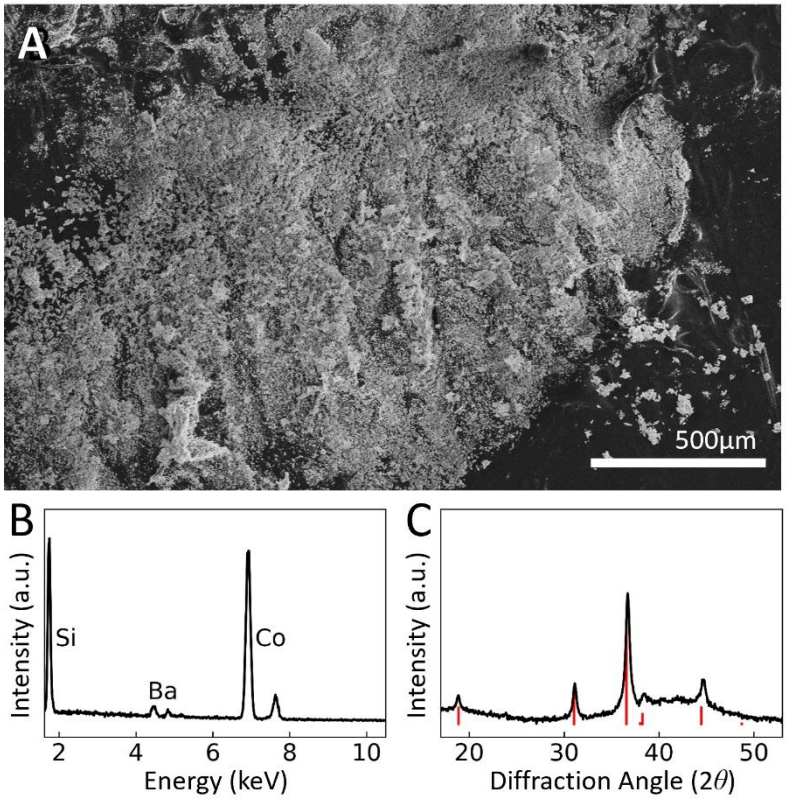

Figure S8. A. SEM of composites grown on the meniscus. It should be noted that these composites need to be crushed into a piece of carbon tape to avoid contamination of the electron microscope and hence have lost their 3D morphology **B.** EDS and **C.** XRD of the composites.

S12. Catalysis Setup

The catalysts were tested for the FTS at 20 bar, 220ºC, H_2/CO = 2/1 and GHSV =320 $mL g_{cat}^{-1} min^{-1}$. Figure S9 shows the experimental set-up used for the FTS experiments. The nanocomposite catalysts (160 mg) were diluted with SiC (1:6) and located in a 10 mm diameter Hastelloy reactor. Above the catalysts and next to the reactor inlet, a bed of SiC was placed to ensure the gases pre-heaten. The reactor was placed in an oven (Carbolite Gero) and the temperature was measured with a thermocouple at the reactor exit and one thermocouple inserted in the SiC bed. The liquid products are collected in a hot-trap at the reactor exit, while the gases flown through a heated line at 250°C, towards the gas chromatograph (Trace 1300, Thermo Fisher Scientific).

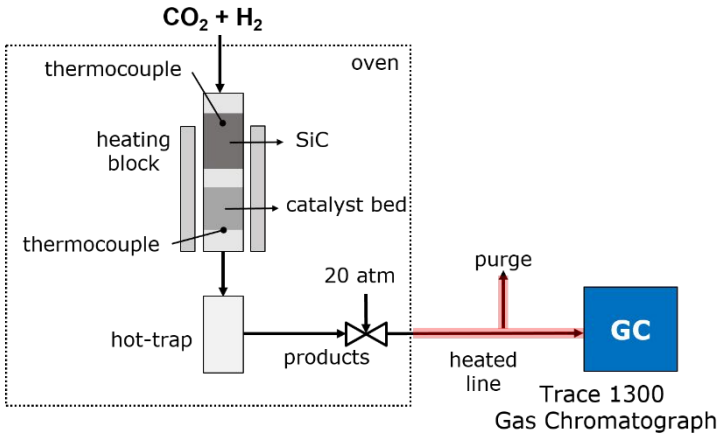

Figure S9. Experimental set-up for the FTS.

The gas chromatograph contains two TCD and two FID detectors. One line (columns MXT-1 and MXT-QBond), connected to a FID detector, is used to quantify the short hydrocarbons (C_1-C_3); and CO_2 in a TCD detector. In the second line (column RTX-1) the long hydrocarbons (C_4-C_{25}) are analyzed in an FID detector. The permanent gases are quantified using a TCD detector.

The BET surface area and pore distribution of the Co_3O_4/SiO_2 nanocomposite was measured by Micromeritics Tristar II, showing a S_{BET} of 36.3 m^2/g and an average pore size of 6.6 nm.

The TOF was computed using a well-established method (A. Martínez, C. López, F. Márquez, I. Díaz, *J. Catal*, **2003**, 220, 486-499). The approach that we use in the manuscript is a well-established method to compute the TOF for the FTS. The particle size of the metallic Co (d_{Co}) is computed form the particle size of the Co3O4 ($d_{Co_3O_4}$) precursor as d_{Co}= 0.75 $d_{Co_3O_4}$, which enables computation of the TOF following:

$$TOF = \frac{R_{CO} M_{Co}}{(D)(L)}$$

where, R_{CO} is the reaction rate by mass of catalyst, M_{Co} is the Cobalt molar mass, L is the cobalt loading, D is the cobalt dispersion calculated as (A. Borodzinski, M. Bonarowska, Langmuir, **1997**, 13, 5613-5620):

$$D(\%) = \frac{2.64}{\left(d_{Co}/d_{at}\right)^{0.81}}$$

where d_{at} is the Cobalt atomic diameter.

S13. IR Measurements

The IR spectra were recorded using a Bruker Vertex 80v FT-IR spectrometer equipped with an ATR module (Platinum ATR Diamond) by first measuring a background after 40 minutes to flush water vapor and CO_2 out and then measuring the converted nanocomposites after a similar 40 minutes wait time.

From the IR spectrum (Figure S10), the presence of $Co(CO_3)_x(OH)_{2-2x}$ after the cation exchange was investigated. First, the presence of a carbonate anion was confirmed with the fingerprint peak at 1400 cm^{-1}. Furthermore, a broad peak at 3300-3400 cm^{-1} was observed, which indicates hydrogen bonded hydroxyl groups, while the absence of peaks around 3800 cm^{-1} indicates no unbound hydroxide groups are present. Furthermore, the absence of a large peak at 1645 cm^{-1} omits the possibility of large amounts of water present in the sample. These observations lead to the conclusion that basic cobalt carbonate has formed, especially as the observed spectrum is in good agreement with the IR spectra of basic $Co(CO_3)_x(OH)_{2-2x}$ found in literature (Nassar and Ahmed, *Polyhedron*, **2011**, *30,* 2431-2437).

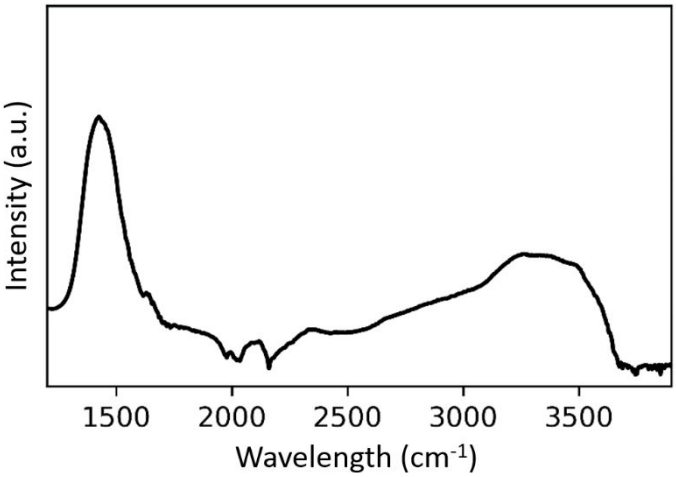

Figure S10. IR-spectrum of the amorphous $Co(CO_3)_x(OH)_{2-2x}$ nanocomposites. The peak around 1400 cm^{-1} indicates the presence of a carbonate anion, whereas the bump around 3300-3400 cm^{-1} shows the presence of OH-groups.